ANNALS of the ORADEA UNIVERSITY.
Fascicle of Management and Technological Engineering, Volume VI (XVI), 2007

OPTICAL FIBER PHOTONIC EMBEDDED SENSOR

Roxana-Mariana BEIU, Constantin D. STANESCU
University “Politehnica” of Bucharest

Abstract. This paper details a novel enabling fiber optic sensor based on photonic crystal structures embedded in the core of the fiber. We will start by briefly introducing fiber optics as well as presenting their application for sensing mechanical deformations. Afterwards we review some of the main features of photonic crystals, and detail the geometry of a photonic crystals sensor embedded in an optical fiber. We will show the changes of the electromagnetic field components due to variations of the sensor’s geometry, and evaluate its overall sensitivity. Simulation results will support our claim that embedded photonic crystals can be used for sensing very small mechanical deformations.

1. INTRODUCTION

The enduring trend towards miniaturization has lead to many new theoretical advancements and has enabled countless applications in electronics, optics, and fine mechanics. These fields are now coming together allowing us to envisage the development of new sensors—as well as novel ways of processing and communicating information. Currently, fiber optic (FO) based systems play a major role in communications, but the particular qualities they posses makes them a very attractive candidate for both sensing and processing information.

A photonic crystal (PC) is a regular (modulated dielectric) structure, with a periodicity comparable to that of the input wavelength. PCs exhibit very strong interaction with light. They present peculiar characteristics, as light interacts with them in ways completely different from what is knows from classical optics, including inhibition of light transmission (inside the PC), and photonic band gap (PBG) formation. Such phenomena can be used in modern information transmission and processing systems, and in sensory devices.

In this paper we will show that embedding PC structures into standard monomode FOs allows for highly sensitive detection of mechanical deformations. The paper starts by reviewing some of the characteristics of FOs and PCs. Afterwards we shall present the new FO sensor geometry and the material characteristics. The simulation results will reveal both the transversal electric (TE) and magnetic (TM) components of the electromagnetic field. These simulations will show both the amplitude and the phase, and have been obtained using EMExplorer (a CAD tool for electromagnetic field computation). Many simulations have been performed at various loading forces (ranging from 0 N to 10 N), allowing us to identify sharp phase variations of TM. These could be used to detect mechanical deformations down to tens of picometers. Conclusions and further directions of research are ending the paper.

2. FIBER OPTIC SENSORS FOR MECHANICAL DEFORMATION

During the ‘80, optical communication through FOs evolved from a curiosity into a dominant technology [1]–[4]. Some of the advantages of FOs are: immunity to electromagnetic noise, capability of sending signals over long distances (low attenuation), lighter weigh, higher signal quality, and greater information capacity.

Besides their use in communications, FOs have found a promising field in sensing [5]–[8]. A particular but important subclass of FO sensors is represented by those used for detecting small mechanical deformations. Initially, the FO deformation sensors were designed like the resistive ones: the geometrical variation (ΔL, also known as deformation

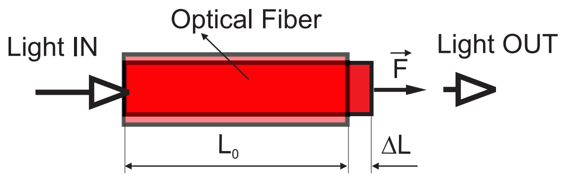

Fig. 1. Mechanical deformation sensing principle for a FO sensor device; $\vec{F}$ ***is the loading force, while*** ΔL ***is the deformation (elongation).***

or elongation) being measured by changes in light transmission between input and output (Fig. 1).

Currently, many novel FOs sensing methods have been discovered. Among these the following ones are used for measuring small mechanical deformations:

– Fiber Bragg grating (FBG) - which couples the forward propagating core mode to the backward propagating core mode [9]–[14];
– Long-period fiber grating (LPG) - which couple the forward propagating core mode to one, or a few, of the forward propagating cladding modes [15];
– Fabry-Pérot (FP) fiber sensor - which uses the FO in an interferometric (FP) setting for sensing very small mechanical deformations [16]–[20].

The fiber grating (FBG, LPG) sensors are the most widely used ones for strain and temperature FO sensing devices.

3. PHOTONIC CRYSTALS

The electromagnetic phenomena inside PCs were discovered simultaneously by Yablonovitch [21], and John [22] in 1987. Since then, there have been many papers published on this topic [23]–[37], with a forthcoming review on 3D PCs illustrating their main characteristics [38]. Meanwhile, the technological capabilities (borrowing from integrated circuits) for the fabrication of advanced micro/nano-structures have constantly been improving, leading to a plethora of fabrication recipes.

Inside PCs two main scattering phenomena are taking place [35]:

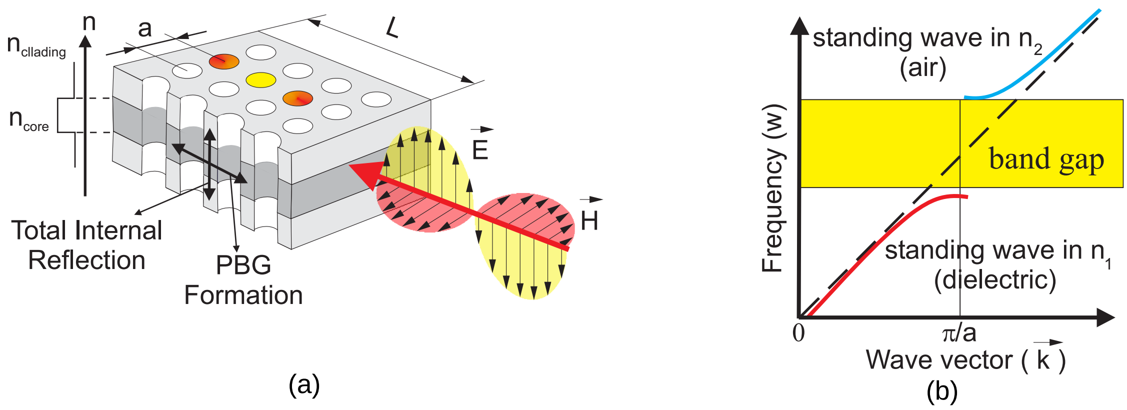

Fig. 2. Wave traveling through a 2D PC structure: (a) PC's air holes in a ridge waveguide; and (b) Formation of the PBG. Here $\vec{H}$ ***, and*** $\vec{E}$ ***are the magnetic and respectively the electric component of the electromagnetic field, a is the lattice periodicity, and n represent the refractive index.***

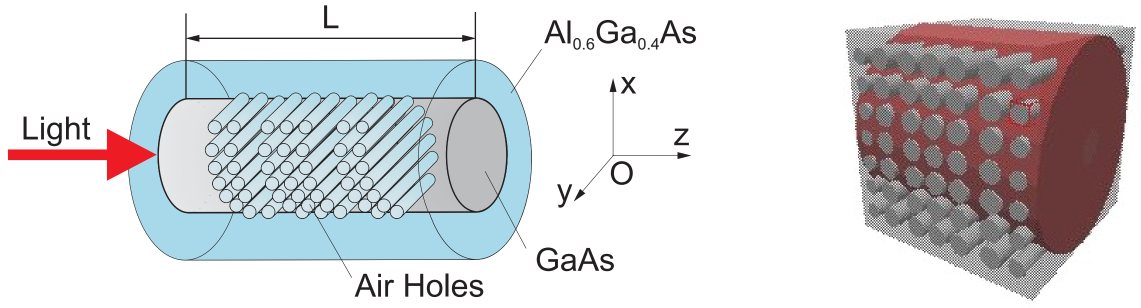

Fig. 3. a) Schematic view of the optical fiber photonic crystal embedded sensor; b) the structure as appear in EMExplorer geometry setup.

- the Bragg (macroscopic) scattering resonance occurring in a periodic structure;
- the Mie (microscopic) scattering resonance from a single unit cell (occurring at the maximum backscattering).

The propagation of light through a ridge waveguide (Fig. 2(a)) is having two main aspects: the guidance of light due to the total internal reflection on one dimension (Oz) as in any FO, and due to the formation of PBG on the other two dimensions Ox and Oy. As we can see from Fig. 2(b), the PBG occurring in such a structure defines three main bands: upper, mid-gap (highlighted in yellow), and lower. Each one represents a frequency domain where light is interacting with the PC (made of dielectric and air interstitials). The lower band is represented by those frequencies corresponding to propagation through dielectric (having high refractive index). The upper band corresponds to air light propagation (having low refractive index).

The main characteristic of a PC structure is its periodicity *a.* The associated PBG size ($\Delta\omega$) can be determined from the refractive index contrast, defined by $\left(n_1^2 - n_2^2\right)/2n_1^2$, and the filling ratio *f* of the higher index material (i.e., the relative amount of material composing the scattering PCs structure over the total volume of the PC). Meanwhile, the location of the mid-gap frequency (ω_m) is determined by the lattice constant *a* of the PC (Fig. 2(b)). Finally, one more important aspect is the scaling of the PBG: if the PC is scaled by a factor *s*, all frequencies (upper and lower bands, as well as mid-gap one) will be scaled by *s*, but the ratio gap/mid-gap ($\Delta\omega/\omega_m$) remains the same [39]. By a smart engineering of the PC's geometry it is possible to control light (i.e., amplify or inhibit it in a desired way).

4. A NEW PHOTONIC SENSOR

We have chosen a monomode FO (see Fig. 3) having the core and the cladding made of GaAs, and $Al_{0.6}Ga_{0.4}As$ respectively. We decided to embed a PC in the FO as shown in Fig. 3. The geometrical dimensions of the PC structure a, b, ϕ_1, ϕ_2 are detailed in Table 1. These have been taken from [40]. This PC was chosen due to the fact that in [40] it is shown that a 1 nm elongation (ΔL) would correspond approximately to a 1.5 nm shift in the peak transmission wavelength [40]. It is worth mentioning that, for both FO materials used, the absorption index *k* is equal to zero at λ = 1.5 μm [41].

Table 1. Optical and geometrical values for the embedded PC.

λ [μm]	$n_{Al0.6Ga0.4As}$	n_{GaAs}	L [μm]	ϕ_1 [μm]	ϕ_2 [μm]	a [μm]	b [μm]	Y [N/m^2]
1.5	3.073	3.4	3	0.304	0.234	0.386	0.490	8.53*10^{10}

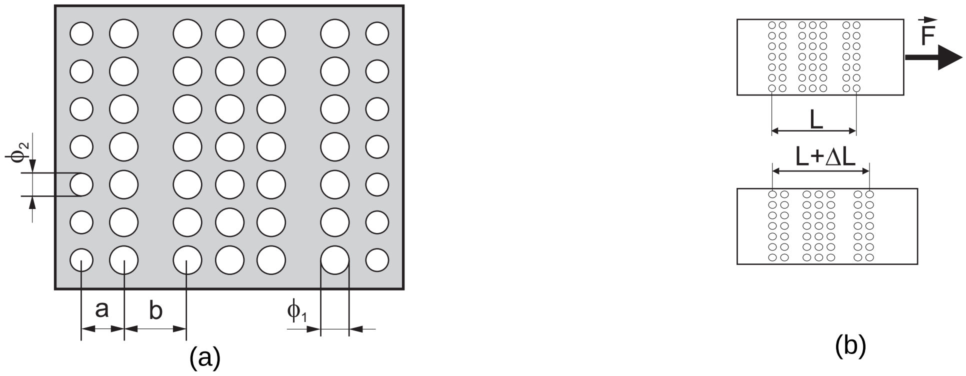

Fig. 4. (a) A section through the PC (air holes) embedded in the FO; a, b, ϕ_1, ϕ_2 are elementary geometrical dimensions; and (b) The deformation of the embedded PC (of length L) under a force F.

In general, for an $Al_xGa_{1-x}As$ alloy, Young's modulus can be calculated as [42]:

$$Y(x) = (8.53 - 0.18x)\cdot 10^{10}\ [\mathrm{N/m^2}] \tag{1}$$

In our simulation we have used $Y_0 = 8.53\times10^{10}$ N/m^2 as the core of the FO is of GaAs.

The square grid PC embedded in the FO (see Fig. 4a)) is characterized by *a*, *b*, ϕ_1, ϕ_2. The air holes have diameter ϕ_1, while ϕ_2 is the diameter of the first and the last row only (23% less then ϕ_1). The holes are placed at a distance of *a*, with the exception of the third and sixth columns, which are placed at a distance *b*.

If a force *F* is applied to the system (as in Fig. 4(b)), an elongation ΔL appears. We can compute ΔL from Hook's law:

$$Y = \sigma/\varepsilon,\ \sigma = F/A,\ \varepsilon = \Delta L/L,\ \text{hence } \Delta L = LF/A/Y \tag{2}$$

where σ is the stress due to mechanical deformations, ε is the strain (a relative measure of deformation), and *A* is the area. The force *F* will also affect the elementary dimensions of the PC: *a*, *b*, ϕ_1, ϕ_2. Table 2 shows one example for *F* = 1 N. We have used Excel to generate a new set of data for each different value of *F* in the range 0 to 10 N. L_0, R_0, and A_0 are the initial length, radius, and respectively cross sectional area of the FO. The column labeled *X* gives the positions of the holes' centers (on the Oz direction). By changing *F* we obtain the new $X + \Delta X$ values as centers. These have been inputted in EMExplorer as the new air holes positions.

As can be seen from Table 2, the elongation of the FO loaded by 1 N is 4.48 nm. A

Table 2. Altered geometrical dimensions for a given elongating force.

***Y* [N/m^2]**	***L_0* [μm]**	***F* [N]**	***R_0* [μm]**	***A_0* [m^2]**	**Δ*L* [nm]**
8.530×10^{10}	3.000	1.000	50.000	7.854×10^{-9}	4.48

***a* [nm]**	***b* [nm]**	***X* [nm]**	**Δ*X* [nm]**	***X* + Δ*X* [nm]**
386	490	238	0.0000	238.0000
		624	0.5762	624.5762
ϕ_1[nm]	**ϕ_2[nm]**	1114	1.3076	1115.3076
304	234	1500	1.8837	1501.8837
		1886	2.4599	1888.4599
		2376	3.1913	2379.1913
		2762	3.7675	2765.7675

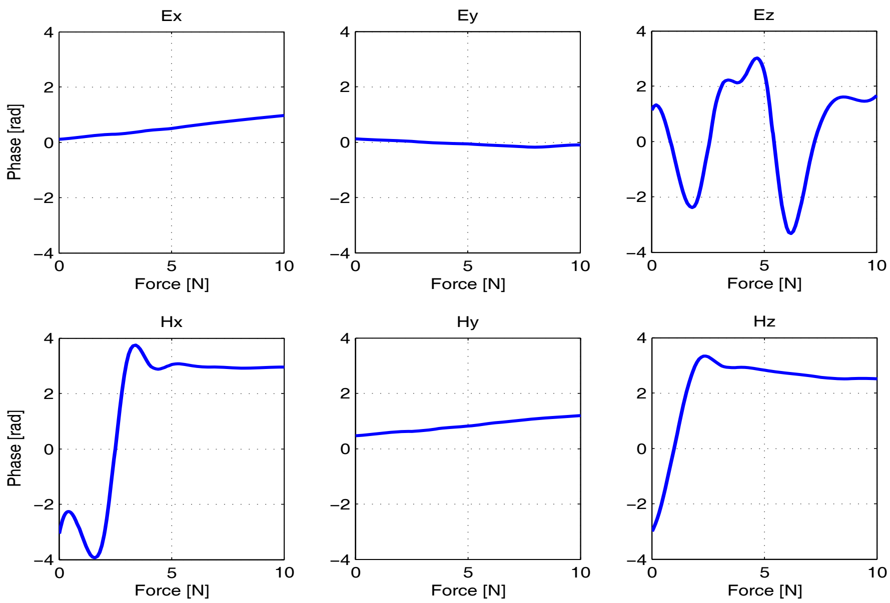

Fig 5. The $\vec{E}$ and $\vec{H}$ phase variations during fiber elongation.

1 nm elongation (ΔL) should correspond to about 1.5 nm shift in the peak transmission wavelength [40]. It follows that such a system could in principle exhibit a wavelength shift of about 4.48×1.5 = 6.72 nm.

5. SIMULATION RESULTS

All the simulations presented here were done using EMExplorer v3.0 [43] running on a PC at 3.73 GHz and with 16 GB of RAM. One calculation takes about 48 hours, due to the high 3D sampling of the sensor's volume (3×3×3 μm^3). The input source is a 1.5 μm plane wave on the Oz axis (see Fig. 3). The amplitude and phase of the electromagnetic field components (E_x, E_y, E_z, H_x, H_y, H_z) for different FO deformations between 0 N and 10 N are reported in Fig. 5 (phase) and Fig. 6 (amplitude). From these plots we can see that two

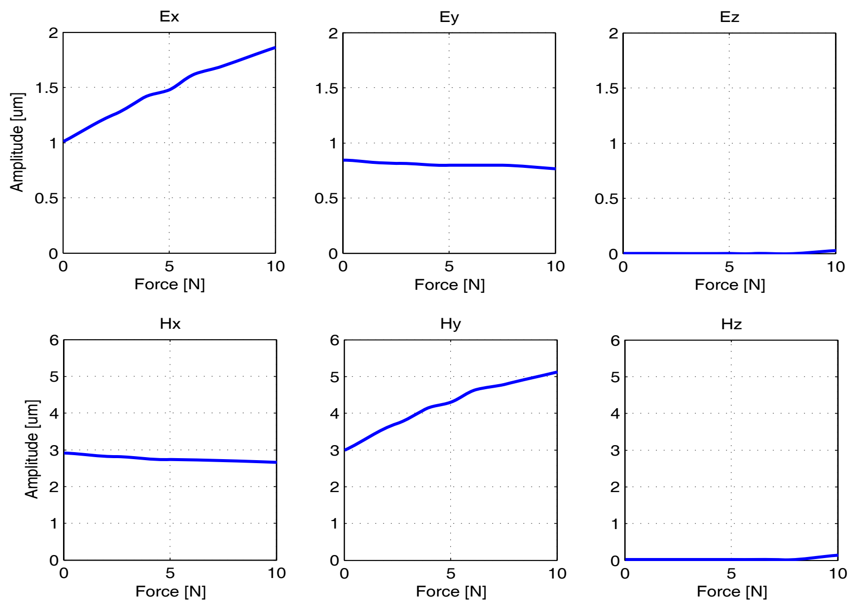

Fig. 6. The $\vec{E}$ and $\vec{H}$ amplitude variations during fiber elongation.

of the $\vec{H}$ phase components, namely H_x and H_z, present quite sharp transitions for only a 1 N (or less) force variation. From Fig. 5, the variation of H_x phase is from –3.134 to +3.075 radians for a force variation of 1 N (from 2 N to 3 N). This means that a sensor like the one presented in Fig. 3 could use the H_x phase to sense a mechanical deformation of ΔL=4.48 nm (corresponding to 1 N) while having a phase variation of 3.075 – (–3.134) = 6.25 radians. This corresponds to a phase change of 358°, leading to a sensitivity of about 4.48nm/358° = 0.0125 nm/°. This suggests that the sensitivity of such sensors could be in the tens of pico-meter range.

6. CONCLUSIONS

FO sensory systems are not only an extremely wide-ranging area, but also a far-reaching and very generous one. It covers both theoretical discoveries and R&D advancements, as well as enabling fabrication methods and sophisticated measurement techniques.

The discovery of regular structures known as PCs has led to a sustained research effort. This has revealed peculiar PC characteristics—based on PBG formation. This allows us to envision numerous practical applications among which the most promising and rewarding ones are: embedded optical sensors, (future) on-chip optical communications and (even) optical computations.

This paper has detail a new sensory system based on a PC embedded in a monomode FO. Simulations have shown that measuring the output phase of TM components can provide information about mechanical deformations with an accuracy in the tens of pico-meters range.

BIBLIOGRAPHY

1. G. Snell, “An Introduction of Fiber Optics and Broadcasting,” SMPTE J., vol. 105, 1996, pp. 1–7.
2. H.J.R. Dutton, “Understanding Optical Communications,” Intl. Tech. Support Org., 1998 [available at www.redbooks.ibm.com/pubs/pdfs/redbooks/sg245230.pdf].
3. J. Reinhard, “Fundamentals of Fiber Optics,” Volpi Manufacturing Tech. Rep., 2000 [available at https://www.machinevisiononline.org/public/articles/Volpi_FiberOpticsRevAa.PDF].
4. C. Yeh, “Handbook of Fiber Optics. Theory and Applications,” Academic Press Inc., San Diego, CA, USA, 1990.
5. B. Lee, “Review of the Present Status of Optical Fiber Sensors,” Optical Fiber Tech., vol. 9, 2003, pp. 5779.
6. K.S.C. Kuang, S.T. Quek, and M. Maalej, “Assessment of an Extrinsic Polymer-Based Optical Fibre Sensor for Structural Health Monitoring,” J. Meas. Sci. Tech. vol. 15, 2004 pp. 2133–2141.
7. C. Gorecki, “Sub-Micrometric Displacement Meassurements by an All-Fiber Laser Heterodyne Interferometer Using Digital Phase Demodulation,” J. Optics, vol. 26, 1995, pp. 29–34.
8. S.K. Ghorai , D. Kumar, and B. K Hura, “Strain Measurement in a Mach-Zehnder Fiber Interferometer Using Genetic Algorithm,” Sensors & Actuators A, vol. 1, 2005, pp. 215–221.
9. P.M. Cavaliero, F.M. Araujo, L.A. Ferreira, J.L. Santos, and F. Farahi, “Simultaneous Measurement of Strain and Temperature Using Bragg Gratings Written in Germanosilicate and Boron-Codoped Germanosilicate Fibers,” IEEE Photonics Tech. Lett., vol. 11, 1999, pp.1635–1637.
10. H.K. Kang, H.J. Bang, C.S. Hong, C.G. Kim, “Simultaneous Measurement of Strain, Temperature and Vibration Frequency Using a Fibre Optic Sensor,” J. Meas. Sci. Tech., vol. 13, 2002, pp. 1191–1196.
11. X. Li, and F. Prinz, “Metal Embedded Fiber Bragg Grating Sensors in Layered Manufacturing,” J. Manufacturing Sci. & Eng., vol. 125, 2003, pp. 577–585.
12. E. Chehura, C.C. Ye, S.E. Staines, S.W. James, and R.P. Tatam, “Characterization of the Response of Fibre Bragg Gratings Fabricated in Stress and Geometrically Induced High Birefringence Fibres to Temperature and Transverse Load,” Smart Mat. Struct. vol. 13, 2004, pp. 888–895.
13. O. Frazão, J.P. Carvalho, L.A. Ferreira, F.M. Araújo, and J.L. Santos, “Discrimination of Strain and Temperature Using Bragg Gratings in Microstructured and Standard Optical Fibres,” J. Meas. Sci. Tech., vol. 16, 2005, pp. 2109–2113.

14. P. Moyo, J.M.W. Brownjohnb, R. Sureshc, and S.C. Tjinc, “Development of Fiber Bragg Grating Sensors for Monitoring Civil Infrastructure,” J. Eng. Struct., vol. 27, 2005, pp. 1828–1834.
15. S.W. James, and R.P. Tatam, “Optical Fibre Long-Period Grating Sensors: Characteristics and Application,” J. Meas. Sci. Tech., vol. 14, 2003, pp. R49–R61.
16. J. Sirkis, T. A. Berkoff, R. T. Jones, H. Singh, A. D. Kersey, E. J. Friebele, and M. A. Putnam, “In-Line Fiber Etalon (ILFE) Fiber-Optic Sensors,” J. Ligthwave Tech., vol. 13, 1995, pp.1256–1263.
17. C.-C. Chang, and J. Sirkis, “Multiplexed Optical Fiber Sensors Using a Single Fabry-Perot Resonator for Phase Modulation,” J. Lightwave Tech., vol. 14, 1996, pp. 1653–1663.
18. V. Bhatia, M.B. Sen, K.A. Murphy, and R.O. Claus, “Wavelength-Tracked White Light Interferometry for Highly Sensitive Strain and Temperature Measurements,” Electr. Lett., vol. 32, 1996, pp. 247–249.
19. D. Johlen, P. Klose, H. Renner, and E. Brinkmeyer, “Fiber Fabry-Perot Interferometer with Mode-Converting Bragg Gratings,” J. Ligthwave Tech., vol. 18, 2000, 1575–1582.
20. J.-Y. Rao, “Recent Progress in Fiber-Optic Extrinsic Fabry-Perot Interferometric Sensors,” Optical Fiber Tech., vol. 12, 2006, pp. 227–237.
21. E. Yablonovitch, “Inhibited Spontaneous Emission in Solid-State Physics and Electronics,” Phys. Rev. Lett., vol. 58, 1987, pp. 2059–2062.
22. S. John, “Strong Localization of Photons in Certain Disordered Dielectric Superlattices,” Phys. Rev. Lett., vol. 58, 1987, pp. 2486–2489.
23. E. Özbay, E. Michelm, G. Tuttle, R. Biswas, M. Sigalas, and K.-M. Ho, “Micromachined Millimeter-Wave Photonic Bandgap Crystals,” Appl. Phys. Lett., vol. 64, 1994, pp. 2059–2061.
24. C.T. Chan, S. Datta, K.-M. Ho, and C.M. Soukoulis, “A7 Structure: A Family of Photonic Crystals,” Phys. Rev. B, vol. 50, 1994, pp. 1988–1991.
25. S. Fan, R.F.L. Villeneuve, R.D. Meade, and J.D. Joannopoulos, “Design of Three-Dimensional Photonic Crystals at Submicron Lengthscales,” Appl. Phys. Lett., vol. 65, 1994, pp. 1466–1468.
26. J.D. Joannopoulos, R.D. Meade, and J.N. Winn, “Photonic Crystals: Molding the Flow of Light,” Princeton Univ. Press, 1995.
27. J.D. Joannopoulos, “The Almost-Magical World of Photonic Crystals,” Brazilian J. Phys., vol. 26, Mar. 1996, pp. 58–67.
28. J.D. Joannopoulos, P.R. Villeneuve, and S.H. Fan, “Photonic Crystals,” Solid State Comm., vol. 102, 1997, pp. 165–173.
29. A. Chutinan, and S. Noda, “Spiral Three-Dimensional Photonic-Band-Gap Structure,” Phys. Rev. B, vol. 57, 1998, pp. R2006–R2008.
30. Y.A. Vlasov, K. Luterova, I. Pelanta, B. Hönerlage, and V.N. Astratov, “Optical Gain and Lasing in a Semiconductor Embedded in a Three-Dimensional Photonic Crystal,” J. Cryst. Growth, vol. 184-185, 1998, pp. 650–653.
31. S. Noda, “Three–Dimensional Photonic Crystals Operating at Optical Wavelength Region,” Phys. Rev. B, vol. 279, 2000, pp. 142–149.
32. V. Mizeikis, S. Juodkazis, A. Marcinkevicius, S. Matsuo, and H. Misawa, “Tailoring and Characterization of Photonic Crystals,” J. Photochem. & Photobiol. C: Photochem. Rev., vol. 2, 2001, pp. 35–69.
33. E. Yablonovitch, “Photonic Crystals: Semiconductors of Light,” Sci. Amer., vol. 285, 2001, pp. 47–55.
34. O. Toader, and S. John, “Square Spiral Photonic Band Gap Crystals: Robust Architecture for Microfabrication of Materials with Large Three-Dimensional Photonic Band Gaps,” Phys. Rev. E, vol. 66, 2002, pp. 016610 (1–18).
35. S. John, O. Toader, and K. Busch, “Photonic Bandgap Materials: A Semiconductor for Light,” Encyclopedia of Physical Sci. & Tech., vol. 12, 2002, Academic Press, pp. 133–145.
36. C. López, “Materials Aspects of Photonic Crystals,” Adv. Mat., vol. 15, 2003, pp. 1679–1704.
37. C. López, “Photonic Crystals: Fundamentals and Applications,” IEEE Electr. Dev. Meeting, IEDM Tech. Digest, 2004, pp. 359–362.
38. R.M. Beiu, C.D. Stanescu, A. Carstoiu, “On 3D Photonic Crystals: A Brief Evaluation of Their Main Characteristics for Various Topologies,” UPB Sci. Bull., 2007, under review.
39. M. Woldeyohannes, and S. John, “Coherent Control of Spontaneous Emission Near a Photonic Band Edge,” J. Opt. B: Quant. Semiclass. Opt., vol. 5, 2003, pp. R43–R82.
40. A.S. Jugessur, P. Pottier, and R.M. de la Rue, “Engineering the Filter Response of Photonic Crystal Microcavity Filters,” Optics Express, vol. 12, 2004, pp. 1304–1312.
41. http://www.ioffe.ru/SVA/NSM/nk/index.html
42. S. Adachi, “GaAs, AlAs, and $Al_xGa_{1-x}As$: Material Parameters for Use in Research and Device Applications,” J. Appl. Phys., vol. 58, 1985, pp. R1–R29.
43. www.emexplorer.net